Routing stemflow water through the soil: a dual labelling approach with artificial tracers

Juan Pinos[1,2], Markus Flury[2], Jérôme Latron[1], Pilar Llorens[1]

[1]Surface Hydrology and Erosion Group, Institute of Environmental Assessment and Water Research, IDAEA-CSIC, Barcelona, Spain
[2]Department of Crop and Soil Sciences, Washington State University, Puyallup, WA 98371 and Pullman, WA 99164, USA

Correspondence to: Juan Pinos (juan.pinos@idaea.csic.es)

Abstract. Few studies have explored the stemflow double-funnelling phenomenon, although subsurface flow along roots and macropores plays a significant role in determining hydrological responses in forested catchments. In this study, a stemflow experiment on *Pinus sylvestris L.* (Scots pine) used artificial tracers to view and quantify the preferential flow of stemflow water after infiltration into the soil. Forty-one litres of water labelled with enriched deuterium and Brilliant Blue FCF were applied at a flow rate of 7 L h^{-1} to the stem of a pine tree, which corresponds to stemflow caused by about 50 mm rainfall. TDR probes were distributed around the tree trunk and in depth profiles to measure high-resolution volumetric water content. One day after the stemflow discharge, soil pits were dug in the different cardinal directions and at varying distances from the tree. Photographs were taken for imaging analysis to quantify preferential flow metrics. Soil samples were taken from the different profiles to analyse dye concentrations and isotopic compositions. We found that stemflow infiltrated through an annulus-shaped area around the tree base. We observed a heterogenous spatiotemporal soil moisture response to stemflow and the occurrence of shallow perched water tables around the tree trunk. Dye staining demonstrated that stemflow infiltrated primarily along the surface of coarse roots and also through macropores. The dye coverage was less extensive close to the soil surface and increased with depth and with proximity to the tree trunk. Lateral flow was also observed, mainly in the shallow soil layers. A set of metrics demonstrated the prevalence of preferential flow. Deuterium and Brilliant Blue FCF concentrations correlated with each other significantly. The concentrations decreased at increasing distance from the tree trunk, indicating dilution and mixing with residual soil water. Macropores, coarse roots (living or decayed) and perched water tables produced a complex network regulating the preferential flow. Our results suggest that stemflow heavily affects soil moisture distribution, and thus also groundwater recharge and surface runoff. Our study provides insights into the physical processes controlling stemflow belowground funnelling and improves our understanding of forest-water interactions.

1 Introduction

Stemflow is the proportion of rain intercepted by the tree canopy that is channelled towards the bole and eventually flows downward and infiltrates into the forest floor around the stem base. Stemflow contributes higher amounts of water and solutes in near-stem soils than the throughfall contribution in the rest of the forest (Carlyle-Moses et al., 2018). Stemflow varies widely across vegetation types and climatic regions (Levia and Frost, 2003; Llorens and Domingo, 2007; Yue et al., 2021). Recent research has unveiled biotic and abiotic factors that regulate stemflow production before it is funnelled belowground (Levia and Germer, 2015; Cayuela et al., 2018; Zhang et al., 2021). Although stemflow is not a major proportion of the overall catchment water balance, it can saturate near-stem soil and may enhance overland, preferential or subsurface flow, contribute to soil water replenishment and groundwater recharge, produce soil erosion (Levia and Germer, 2015), transport chemical, particulate and biological materials (Van Stan et al., 2021), and influence root water uptake (Hildebrandt, 2020). Due to its importance in soil hydrology, biogeochemistry and ecohydrology, stemflow has become an active topic of research in recent years (see Levia et al., 2011; Van Stan et al., 2020).

A key topic in stemflow research is root-induced bypass flow, introduced by Johnson and Lehmann (2006) as the "double-funnelling of trees". This term refers to the process whereby a first aboveground funnelling occurs when rainfall turns into stemflow, followed by a second belowground funnelling in which stemflow is led into the soil along tree roots and macropores through an unsaturated soil matrix.

While the concept of the double-funnelling phenomenon is well known, clarification of the underlying mechanisms is more challenging. Several experimental techniques, both invasive and non-invasive ones, have been used to study the double-funnelling processes of trees. The most common approaches are the monitoring of water fluxes by soil moisture sensors, the viewing of preferential flow paths by dye tracers, or a combination of the two (Liang et al., 2011; Schwärzel et al., 2012; Spencer and van Meerveld, 2016; Gonzalez-Ollauri et al., 2020; Tischer et al., 2020). Recently, non-invasive geophysical techniques such as ground-penetrating radar (GPR) and electrical resistivity tomography (ERT) have also been used to study double-funnelling processes (Guo et al., 2020; Di Prima et al., 2022). The majority of these stemflow funnelling studies, of various deciduous and evergreen trees, found that stemflow infiltration leads to vertical and/or horizontal preferential flow along the surface of coarse roots, although matrix stemflow infiltration has been reported as well (Gonzalez-Ollauri et al., 2020).

Despite their potential for the study of water movement in the vadose zone, geophysical techniques often cannot resolve flow pathways at small-scale resolution, which limits their usefulness in stemflow infiltration research (Fan et al., 2020). On the other hand, dye tracing for staining flow pathways has become an established way to show preferential flow in soils (Flury & Wai, 2003). The results obtained from staining experiments clearly illustrate at high spatial resolution the complicated patterns of water movement (Ghodrati and Jury, 1990; Flury et al., 1994; Weiler and Flühler, 2004). However, the disadvantage of staining is that it is a destructive technique that provides only one-off results. Besides, as dyes are adsorbed to some extent by the soil matrix (e.g., Brilliant Blue FCF; Ketelsen and Meyer-Windel, 1999; German-Heins and Flury, 2000), there is a certain degree of underestimation of the flow paths. Therefore, new approaches are needed to unravel the patterns of stemflow belowground funnelling. Stable isotopes, such as deuterium (^{2}H), have been widely use in hydrology as conservative tracers (Kendall and McDonnell, 1998). In combination with dye tracers, they could be a powerful tool for unravelling stemflow double-funnelling phenomena.

In this study, we developed an approach to characterize the double-funnelling process by using high-resolution hydrometric monitoring and dual-tracer labelling (^{2}H and dye). The main goals of our study were to assess stemflow infiltration quantitatively by means of dye concentrations, isotopic compositions and hydrometric data (soil water content), and to view the spatial distribution of preferential flow paths by dye staining. The experiment was conducted in a Mediterranean

ecosystem with pine forest cover, which had not been extensively investigated for stemflow double funnelling. This study is a contribution towards the mechanistic understanding of water infiltration patterns and water-root interactions in forested catchments.

2 Material and methods

2.1 Study site

The research was conducted at the Vallcebre research catchments in Catalonia, Spain, established as hydrological and ecohydrological research sites in 1988 (Llorens et al., 2018). The catchments are located 100 km north of Barcelona, in the south-eastern part of the Pyrenees (42°12'N and 1°49'E). Their humid Mediterranean climate is characterized by a mean annual air temperature of 9.2°C and a mean annual precipitation of 856 mm (for the period 1999-2018). Precipitation is seasonal throughout the year, with spring and autumn the wettest seasons and summer and winter the driest. Nevertheless, summer convective storms also provide significant precipitation. Reference evapotranspiration shows a seasonal pattern with maximum values in summer of up to 6.9 mm d^{-1} and a mean annual rate of 823 mm. In the study area, soils developed over the mudstone lithology have a silty loam and silty clay loam texture and are characterized by a rapid decrease in their hydraulic conductivity at depth (Rubio et al., 2008).

Nowadays, Scots pine forests (*Pinus sylvestris* L.), which arose through afforestation of old agricultural terraces, are the main land cover of the catchment, but small fragments of original oak forests (*Quercus pubescens Willd.*) are also found (Poyatos et al., 2003). An experimental Scots pine forest stand (named Cal Rotes) was delineated within the Can Vila catchment to investigate forest-water interactions. The stand density and basal area is 1,189 trees ha^{-1} and 45.1 m^2 ha^{-1}, respectively. One representative mature pine tree (with a diameter at breast height of 27.3 cm and a basal area of 585.3 cm^2), which had been previously instrumented for stemflow measurement during a 6-month period (Cayuela et al., 2018), was selected for our stemflow double-funnelling experiment.

2.2. Artificial stemflow experiment set-up

To simulate stemflow (Figure 1), the approach of Llorens et al. (2022) was adopted in this study. A flexible PVC plastic tube (internal diameter = 10 mm) was placed around the experimental tree at breast height (1.3 m). As the trunks of pine trees are very rough, the outer bark of the tree was removed to assist the assembly of the tube. The plastic tube was perforated on the inside with 2-mm holes every 4-5 cm, such that the holes were in contact with the trunk surface. To ensure uniform wetting of the stem and to prevent splashing of water, cloths were placed between the bole and the tube. The tube was connected by a Y-shaped tubing connector to a water tank. A stopcock was installed upstream of the Y-shaped tubing connector to regulate and control the flow rate. The stopcock was set to achieve a flow rate of about 7 L h^{-1}

Our system was designed to discharge water from a tank which was located 9 m above and ~35 m away from the trunk, creating a gravity-fed water system. Volumetric soil water-content (SWC, cm^3 cm^{-3} or %) was monitored by sixteen 30 cm-long TDR probes (CS615 probes, Campbell Scientific, Logan, UT, USA). The probes were placed vertically in two circular rings, 10 and 20 cm from the trunk every 45°, i.e., facing the cardinal and inter-cardinal directions (Figure 1). When a physical obstacle was encountered (e.g., coarse roots or rocks) that did not allow the installation of the probe, the probe was placed as close as possible. The TDR probes were measured every 20 s and averaged at 1 min intervals by a datalogger (Data Taker DT85, Thermo Fisher Scientific Inc., Waltham, MA, USA). They were previously calibrated with long-term manual TDR measurements performed with a Tektronix 1502-C cable tester (Tektronix Inc., Beaverton, OR, USA) at the study plot. In addition, in each main cardinal direction (N, S, E, W), SWC was monitored by 4 TDR probes (CS605 probes, Campbell Scientific, Logan, UT, USA) installed vertically at depths of 0-10 cm, 0-20 cm, 30-40 cm and 30-60 cm (Figure 1). These probes were measured manually every 30 min with a Tektronix 1502-C cable tester.

Two piezometers were placed at 1.7 and 2.0-m depth at 1.6 m from the tree bole in opposite directions (northwest and southeast, respectively), to sample groundwater. Water levels were measured every 20 minutes with dataloggers (Micro-Diver, Van Essen Instruments, Delft, South Holland, Netherlands). Finally, twelve 30-cm deep mini-piezometers were placed at different distances (between 20 and 50 cm from the bole of the tree) in the cardinal and intercardinal directions to sample the soil water

115 in the shallow layer (Figure 1). When a physical obstacle was encountered, the mini-piezometer was placed as close as possible. Water level was measured about every 30 min and water samples were collected for all the piezometers at one-hour intervals throughout the experiment.

Using the tree location as the centre point, a level mesh (4.8 m x 4.8 m with a grid size of 0.2 m) was placed above the ground. As depicted in Figure 1, the mesh was used as a coordinate system to georeference the installed instruments and to characterize

120 the local topography around the tree. The depth to the ground (z) at every mesh intersection was measured, using the mesh level as the reference plane. All z values were corrected to represent the surrounding topography in relation to the tree base ($z = 0$) and a digital elevation model (0.2 m resolution) was interpolated from these data, with the tree base as the reference elevation (Surfer v.18, Golden Software, Golden, CO, USA).

Unlike what was done in other stemflow infiltration studies (e.g., Schwärzel et al., 2012; Llorens et al., 2022), forest litter (4.7

125 ± 2.4 cm thick according to Molina et al., 2019) was not removed from the forest floor around the tree bole before the experiment. This was in order to simulate as closely as possible stemflow infiltration under natural conditions, because pine litter (with considerable amounts of resins, waxes and aromatic oils) can induce various degrees of water repellence (Iovino et al., 2018), which may affect stemflow infiltration.

The stemflow experiment was conducted on 26 May 2021 when the soil had a moderate moisture condition (mean prior

130 volumetric soil water content of ...). During the previous 20 days, only 15 mm of rain was recorded, of which 6.4 mm occurred on 22 May. We applied 41 L of stemflow water labelled with enriched deuterium and Brilliant Blue FCF dye at a low rate of 7 L h^{-1}. This amount of stemflow corresponds to that commonly generated by a 50-mm rainfall event for this particular site. Enriched deuterium (99.96% fractional D abundance; Eurisotop, Cambridge Isotope Laboratories, Saint-Aubin, France) was mixed with the water to obtain a deuterium isotopic composition of ~500 ‰. To calculate the amount of enriched

135 deuterium to be applied, we used the "D-enriched water" Excel spreadsheet by Prof. Alex Sessions of the Division of Geological and Planetary Sciences, Caltech (http://web.gps.caltech.edu/~als/resources). To validate the amount of enriched deuterium added, preliminary mixing tests were performed and a sample of the final mixture was sent for isotopic analysis. Brilliant Blue FCF (Proquimac, Barcelona, Spain) was selected as the dye tracer because of its favourable physicochemical and toxicological characteristics (Flury and Flühler, 1995). The dye shows a Langmuir-type of sorption behaviour in soil

140 (German-Heins and Flury, 2000). Thus, the higher the concentration, the less relative sorption is expected, as sorption sites become saturated with the dye tracer. In our experiment, a Brilliant Blue FCF concentration of 5 g L^{-1} was used.

2.3. Stemflow infiltration area

Just after the experiment was finished, litter was carefully removed from the surrounding area of the tree base and the stemflow infiltration area (m^2) was determined, following Llorens et al. (2022), by placing a plastic mesh over the soil surface, counting

145 the total number of grid areas covering dye-stained soil and multiplying by the grid-square area (1.27 cm^2 grid square^{-1})

2.4. Plot excavation and soil sampling

One day after the dual-labelled water application, we opened four vertical trenches (30 cm deep and 100 cm wide) in the four cardinal directions at 40 cm distance from the tree bole. Later, two more cross-sections were opened closer to the tree, at a distance of 25 cm and 10 cm in each direction (Figure 2). In total, 12 soil profiles were excavated and photographed throughout

15 the day. The face of each profile was levelled by a steel scraper knife to minimize shadows caused by its unevenness and

roughness. For each of the 12 soil profiles, dye-stained (blue) and non-stained areas were sampled with steel cylinders (100 cm³) to measure dye concentration and isotopic composition. In total, 63 samples were collected and their location georeferenced. Immediately after the samples were taken, they were covered with plastic film and placed into coolers to maintain soil moisture and prevent evaporation, and then transported to the laboratory.

155 **2.5. Image analysis and preferential flow indices**

Because photographs were taken at varying times during the day, with different illumination (shadows vs sunlight), they showed different tints, which made it challenging to analyse colour distribution automatically. Therefore, we used a primary colour scale as a reference to recalibrate the colours and illumination in each photograph (Figure 3a). Then, the saturation of the blue stains was maximized to make it easier to distinguish dye intensities (Figure 3b). The photographs were digitized and 160 edited for geometric correction, contrast and brightness, using Adobe Photoshop 21.2.12 (Adobe Inc., San José, CA, USA).

These corrected images were then used to classify dye-stained and non-stained areas with the maximum-likelihood supervised classification tool in ArcGIS 10.4.1 (Environmental Systems Research Institute Inc., Redlands, CA, USA) (Figure 3c). Identifiable dye-stained and non-stained areas of interest were manually digitized for each image and used as a training set for the classification tool. Unwanted objects were manually masked out to prevent potential inaccuracies in the classification 165 process.

Six preferential flow indices were then derived from the digitized images. These indices were calculated as follows:

Dye coverage (DC, %) (Flury et al., 1994) is the proportion of the dye-stained area to the total area. It was calculated in 10-mm depth increments (dye coverage profile) and for the entire profile (total dye coverage). Total dye coverage is lower when there is a higher degree of preferential flow.

170 **Uniform infiltration depth (UniFr, cm)** (Van Schaik, 2009) is the depth at which the dye coverage decreases below 80%. High values indicate a uniform infiltration process, whereas low values indicate preferential flow.

Preferential flow fraction (PF$_{fr}$, %) (Van Schaik, 2009), defined as the fraction of the total infiltration that flows through preferential flow paths, is calculated as:

$$PF_{fr} = 100 \cdot \left(1 - \frac{UniFr \cdot WP}{TSA}\right) \qquad (1)$$

where WP is the width of the profile (cm), and TSA is the total stained area (cm²).

175 **Length index (LI, unitless)** (Bargués-Tobella et al., 2014) is the sum of the absolute differences between the dye coverage (DC, %) of two consecutive depth intervals i and $i+1$ in a vertical profile of n intervals:

$$LI = \sum_{i=1}^{n-1} |DC_{i+1} - DC_i| \qquad (2)$$

This index is related to the degree of heterogeneity of the dye infiltration pattern, with higher LI values indicating greater preferential flow.

Peak index (PI, unitless) (Bargués-Tobella et al., 2014) is the number of times that the vertical line defined by the total dye 180 coverage intersects the dye coverage profile. This parameter is also related to the heterogeneity of the stained patterns, with high values of the parameter indicating a high degree of preferential flow.

Mass fractal dimension (D$_s$, unitless) (Hatano and Booltink, 1992; Hatano et al., 1992) is related to the basic shape of an object (staining patterns), for example a dot, line or plane. D$_s$ can be derived by fractioning a stained profile into squares

(pixels) of side r (the smallest value of r corresponding to the width of an original pixel), and then counting the number of
185   partially stained squares, $N(r)$. Repetition of this process with increasing r values gives a series of $N(r)$ values. Double
logarithmic plots of $N(r)$ against r show a linear correlation from which D_s is calculated from the slope, as follows:

$$\log N(r) = -D_s \cdot \log r + c \qquad (3)$$

where c is a constant. D_s is calculated in the range of 0 to 2. $D_s = 0$ when the stained pattern is a dot pattern, $D_s = 1$ when it is
a line pattern (long and slender) and $D_s = 2$ when it is the dimension of a completely filled area.

2.6. Dye concentration analysis

190   A similar dye extraction procedure to that of Forrer et al. (2000) was followed. An aliquot of 1 g was taken from the centre of
each soil core on the side corresponding to the soil profile the photographs. Then, this aliquot was mixed with 5 mL of
deionized water, shaken overhead for 3 h, and centrifuged for 30 min at 3,000 rpm (ROTINA 420, Hettich, Kirchlengern,
North Rhine-Westphalia, Germany). The concentration of Brilliant Blue FCF of the supernatant was measured by
spectrophotometry at a wavelength of 630 nm, based on a previously established calibration curve relating absorbance (A) to
195   dye concentration (C_d; mg L^{-1}) ($C_d = 6.83$ A; $R^2 = 0.99$). Because we did not determine the dry mass of the soil cores, the dye
concentration in the soil was then expressed as mass of dye per mass of wet soil (C; mg kg^{-1} of wet soil).

2.7. Isotopic analysis

A sufficient aliquot to fill a test tube (20 mL) was taken from the internal side of each of the 63 core samples. These samples
were sent to the Scientific and Technical Services of the University of Lleida for isotopic analysis. Water from the soil samples
200   was extracted by cryogenic extraction and the stable water isotopes ($\delta^{18}O$ and δ^2H, ‰) were determined by cavity ring-down
spectroscopy (Picarro L2120-i analyser, Picarro Inc., Santa Clara, CA, USA). The equipment had an accuracy of <0.1 ‰ for
$\delta^{18}O$ and <0.4 ‰ for δ^2H, based on the repetition of four reference samples provided by the International Atomic Energy
Agency (IAEA). All isotopic data were expressed in terms of δ values and calculated as follows:

$$\delta = \left(\frac{R_{sample}}{R_{VSMOW}} - 1\right) \cdot 1000 \text{ ‰} \qquad (4)$$

where *VSMOW* is Vienna Standard Mean Ocean Water, and R is the isotope ratio ($^{18}O/^{16}O$ or $^2H/^1H$).

205   **2.8. Soil characteristics**

To characterize the soil at the experimental site, six vertical 30-cm depth profiles were dug on the area where the monitored
tree is located. A depth of 30 cm was the maximum because no relevant changes in soil physical properties had been observed
in similar forest stands in the same study area beyond that depth (Rubio et al., 2008). Tree roots encountered during excavation
were cut and removed. Soil cores were taken with steel cylinders (100 cm^3) in 5-cm depth intervals from the soil surface down
210   to 30 cm, to determine volumetric soil water content (VWC, cm^3 cm^{-3}), bulk density (BD, g cm^{-3}), soil texture, organic matter
content (OM, %) and porosity (ε, %). Once taken, samples were immediately covered with plastic film and placed inside
coolers to maintain sample moisture. Volumetric soil water content and bulk density were determined for each core and the
latter was used to calculate porosity, assuming a particle density of 2.65 g cm^{-3} (Hao et al., 2007). Soil organic matter content
was determined by loss-on-ignition following Wang et al. (2012).

215   For soil texture analysis the protocol described in Faé et al. (2019) was used. The dry soil cores were disaggregated and then
a representative, well-mixed 50 g aliquot was collected from each sample. Gravel (diameter > 2 mm) was removed by sieving.
Then organic matter was removed by use of 15% hydrogen peroxide and clay aggregates were dispersed with sodium
hexametaphosphate. The soil was then sieved through a 50-μm mesh to separate sand-sized particles (0.05 to ⩽ 2 mm). Four

subsamples were taken from the < 50 μm suspension and analysed by laser diffraction (Mastersizer 2000, Malvern Panalytical

220   Ltd., Malvern, Worcestershire, UK). Prior to the analysis, the samples were sonicated for 30 s and instrument parameters were

set to refracting index 1.52, absorption 0.1, stirrer speed 750 rpm, pump speed 1,750 rpm and analysis time 30 s. Finally, the

clay and silt fractions determined by the instrument were averaged after obvious outliers were discarded. The soil texture (sand,

silt and clay fractions) and bulk density were then used to calculate saturated hydraulic conductivity by the Rosett

pedotransfer functions model (Zhang and Schaap, 2017).

225   In addition, to determine the isotopic composition of the soil profile before the experiment (see Section 2.7), disturbed soil

samples were taken in each intercardinal direction from the experimental tree, at a distance of 3 m from the stem. Samples

were taken at the following depth increments: 0-5, 5-10, 10-20, 20-30, 40-50, 90-100 cm.

3 Results and discussion

230   ### 3.1. Soil characteristics

Data obtained from the 30-cm depth profiles were pooled (n=6) to characterize the physical properties of the soil at the forest

stand. Similarly, the isotopic composition values of the four soil cores were also pooled. Figure 4 shows the average ±

standard deviation of the soil properties. Soil texture was classified as silt loam according to the USDA classification. Bulk

density increased from about 1 g cm^{-3} at the topsoil to 1.6 g cm^{-3} at 30-cm depth. Similar bulk density values were observed

235   by Rubio et al. (2008) in the same study area at 50-cm depth. As bulk density values > 1.6 g cm^{-3} affect root growth in silt

loam soils (Zisa et al., 1980), we did not expect root growth or development to be restricted. The increase in bulk density

corresponded to a decrease in saturated hydraulic conductivity, porosity and organic matter content with depth. Soil porosity

decreased by about 24% from topsoil to subsoil, whereas water content at field capacity declined by only about 2%. The high

organic matter content in the topsoil (16%) is due to high amounts of litter on the forest floor, as found by Molina et al. (2019).

240   The δ^{2}H decrease (from -48‰ in the topsoil to -55‰ at 100-cm depth) is due to evaporation, which was also observed by

Sprenger et al. (2019) in the same forest stand.

3.2. Stemflow infiltration area

There are few studies that have used dye tracers to calculate the stemflow infiltration area (see Carlyle-Moses et al., 2020). In

our experiment, stemflow infiltrated into the soil in an annular shape around the base of the tree trunk. The area of the annular

245   shape was 0.14 m^2 which is smaller than the infiltration area of 0.245 m^2 reported by Schwärzel et al. (2012). However, the

other stemflow infiltration areas reported are usually much smaller (e.g., Carlyle-Moses et al., 2018; Tischer et al., 2020;

Llorens et al., 2022). In pine forests there is usually a thick litter layer that repels water (Iovino et al., 2018) and causes the

stemflow infiltration area to expand beyond the immediate vicinity of the tree trunk.

3.3. Soil water content dynamics

250   The spatial distribution of the soil water content around the tree before stemflow initiation was highly heterogeneous, and

remained so during the stemflow experiment (Figure 5). The detailed temporal dynamics of the SWC measured with the

different TDR probes is shown in Figure S1. Heterogeneous volumetric SWC around a tree, induced by stemflow, was also

observed by others (Liang et al., 2011; Tischer et al., 2020). Table 1 shows the pre- and post-stemflow SWC (0 min and 510

min), the maximum SWC peak and the time elapsed until its occurrence for each of the TDR probes.

255   Pre-stemflow SWC showed near-saturated conditions for the southeast and west directions at 30 cm distance from the trunk

(Figure 5, Figure S1, Table 1). These near-saturated conditions explain the lack of response of these TDR probes during the

stemflow experiment. The other TDR sensors, however, responded to the stemflow, as shown by the increase in SWC over

Hydrology and
Earth System
Sciences
Discussions

Open Access

EGU

time (Figure 5, Figure S1). As expected, faster response was observed in the TDR probes closer to the trunk: at 10 cm rather than 30 cm (Figure S1). Nevertheless, the maximum difference in SWC (i.e., difference between the max SWC and the pre-

260   stemflow SWC) was similar at both distances (Table 1). The post-stemflow SWC (~2 h after the end of the experiment) showed a small decrease in soil moisture from peak values, indicating that soil water was gradually percolating to deeper soil horizons while the upper horizon remained at field capacity (Figure S1).

Figure 5 shows that stemflow water was mostly directed to the west-north-east, whereas southwest-south received less. The northeast and northwest locations at 10 cm distance showed the greatest increases in SWC (15 and 16%), while SWC in the

265   southeast and south only increased by 5%. At 30 cm distance, SWC to the north increased by 19%, whereas TDR probes to the southwest and west showed no change in SWC (Figure 5, Figure S1, Table 1). In all those TDR probes that responded to stemflow, the maximum SWC was reached close to the end of the experiment (i.e., around 6 h after initiation of the stemflow).

Our results show that stemflow affects SWC in topsoil even at a distance of 30 cm from the trunk. This finding differs from that of Tischer et al. (2020), who suggested that topsoil water content at a distance of 20 cm from the trunk of a European

270   beech and sycamore maple was mainly driven by throughfall rather than stemflow. On the other hand, Metzger et al. (2017) found that SWC during rainfall events was lower in the immediate vicinity of tree stems than in distal areas due to macropore flow enhancing drainage near the tree trunk. These dissimilarities may be because our study excluded the throughfall contribution and examined only and exclusively stemflow infiltration dynamics. Our study found that, in the absence of throughfall, the SWC responded similarly to stemflow at 10 and 30 cm from the trunk, indicating that lateral flow was occurring

275   even in the shallow soil layers. We found that stemflow was preferentially funnelled belowground through coarse roots (see next section). Thus, lateral stemflow redistribution within the soil was driven by the root architecture of Scots pines, which develops both horizontal (growing in shallow soil layers) and vertical (growing down to deep soil layers) coarse roots, together with their corresponding fine roots (Figure S2).

The dynamics of SWC at different depths also revealed marked differences between the cardinal directions (Figure 6). In

280   general, SWC is greater at depth and surface probes show a more pronounced response to stemflow. However, there may be bypass flow inducing the faster response of deeper probes (Figure 6b, c, d). For instance, in the south profile the TDR probe at 30-40 cm reacted to the stemflow more quickly than the other probes did.

SWC heterogeneity around the tree during the stemflow experiment can be attributed to four factors: (1) preferential flow of stemflow on the trunk itself (as shown in Pinos et al., 2021), (2) preferential flow of stemflow infiltrating into the soil due to

285   the presence of coarse roots that redistribute water flow both vertically and horizontally (Schwärzel et al., 2012), (3) the temporary presence of local perched water tables, and (4) heterogeneous soil structure (Metzger et al., 2017).

3.4. Water table dynamics

Water levels monitored by the mini-piezometers indicated the presence of temporary perched water tables around the tree trunk during the stemflow experiment (Figure 7). Even near-saturated locations (TDR probes swc-SE30 and swc-W30)

290   received stemflow water, as indicated by the occurrence of blue water in nearby mini-piezometers wt-SE20 and wt-W20, respectively (Figure S3). However, no SWC response to stemflow was observed at these locations because the soil was already saturated. Although some of the mini-piezometers were close to TDR probes, the relationship between them showed some inconsistencies. For example, no water was observed in mini-piezometer wt-NW20, located between TDR probes swc-NW10 and swc-NW30, which showed maximum SWC changes of 15% and 7%, respectively. Nor was any water found in mini-

295   piezometer wt-N20 situated close to TDR probes swc-N10 and swc-N30, which showed maximum SWC changes of 11% and 19%, respectively (Table 1). On the contrary, increasing water levels were observed at mini-piezometer wt-S20, which was located near TDR probes swc-S10 and swc-S30, which both had a maximum SWC change of only 5%. However, simultaneous

increases in water levels and SWC were observed for mini-piezometers wt-NE20 and wt-E20 (to a lesser extent) and TDR
probe swc-NE10 and swc-E10, which were close to each other. Mini-piezometers wt-N50, wt-S50 and wt-W50, which were
300 located more than 30 cm from the trunk (Figure 1), did not register any increase in water level. However, mini-piezometer wt-
E50 had a minor increase in water level. Moreover, the groundwater table itself, monitored with northwest and southeast
piezometers (1.7 and 2.0 m deep, respectively) at 1.6 m distance from the tree trunk, did not provide any evidence of change
in groundwater levels (Figure S4). Taken together, piezometer and SWC measurements demonstrated the great temporal and
spatial heterogeneity of the soil-water dynamics of stemflow infiltration.

305 **3.5. Image analysis of stemflow stain patterns and preferential flow paths**

Figure 8 shows the dye coverage for the soil profiles for the different cardinal directions around the tree trunk. Every cardinal
direction shows the same overall trend of greater dye coverage with increasing proximity to the tree trunk. The distribution of
our dye patterns differs from those observed in previous studies of trees at hillslopes (Schwärzel et al., 2012; Spencer and van
Meerveld, 2016), in which dye coverage was found to be lower at the upslope than downslope profiles and a clear downward
310 movement of the dye was seen at increasing distance from the tree. We observed the greatest dye coverage in the immediate
vicinity of the tree (at 10-cm distance), which suggests that the majority of the stemflow infiltration water was directed
vertically. These differences may be related to the fact that our experimental tree is located on a rather flat area with a slope
close to zero.

The metrics to characterize the different dye patterns indicate the prevalence of preferential flow (Figure 8, inserts). The
315 maximum dye coverage observed was less than 30%, highlighting that water flowed through only a small portion of the soil
matrix. The metrics of uniform infiltration depth and the preferential flow fraction indicated the absence of matrix flow (Uni
= 0 cm) and the dominance of preferential flow (PF$_{fr}$ = 100%). The length index (LI) increased with proximity to the trunk and
indicated greater irregularity in the dye patterns and hence increased preferential flow. Similarly, the peak flow metric (PI)
showed irregular stained profiles. However, lower values were observed at 10 cm distance, indicating a less irregular stained
320 pattern. The fractal dimension (D$_s$) of the stained patterns ranged from 1.79 to 1.96, indicating that the preferential flow pattern
occurred in extensive areas (Hatano and Booltink, 1992).

A substantial fraction of bypass and lateral flow occurred along the surface of coarse roots. Living roots can impede flow
locally and change the flow towards soil around the root that is non-compacted and highly conductive. In some of the soil
profiles, stained roots contributed larger areas to the dye patterns than stained soil (Figure 8a north, 8b south, 8c east and west).
325 This pronounced stemflow belowground funnelling along coarse roots is shown in Figure 9. The same phenomenon was
observed in several field studies using dye tracers (e.g., Liang et al., 2011; Schwärzel et al., 2012; Spencer and van Meerveld,
2016; Gonzalez-Ollauri et al., 2020; Tischer et al., 2020) and geophysical techniques (Guo et al., 2020). The dye coverage in
our profiles often showed less coverage in the shallow soil layers (0-15 cm) than at greater depth (Figure 8). This indicates
enhanced bypass flow in the shallow soil layers and increasing dye-matrix interaction in deeper layers. Increased dye-matrix
330 interaction occurs when macropore channels become discontinuous and roots branch out more. This aspect was described by
Van Stiphout (1987) as "Internal Catchment". Moreover, the soil matrix between macropores must be saturated before water
can flow to the next macropore. Although few small stones were found during the excavation, these may influence preferential
flow. We observed that some macropores were intersected by stones and extended dye coverage was found around these stones.

It should be noted that stemflow belowground funnelling could behave differently with other tree species and their associated
335 root-soil systems. For example, Luo et al. (2019) found with dual-tracer experiments that the degree of preferential flow was
greater in coniferous than deciduous forest soil and that roots enhanced preferential flow, showing the important role of tree
species and forest composition on preferential flows in forest ecosystems.

3.5. Dye and deuterium concentrations in soil samples

As expected, the concentrations of both tracers in the preferential flow paths (i.e., the stained areas) were significantly higher
340   than in the surrounding soil matrix (i.e., the non-stained areas). In general, the concentrations of Brilliant Blue FCF and of the
deuterium isotopic composition in the soil samples decreased with distance from the tree ($R^2 = 0.49$ for both tracers; Figure
10). Moreover, the maximum concentrations of both tracers in the different consecutive profiles also decreased with increasing
distance from the trunk (Table S1). The Brilliant Blue FCF concentrations and deuterium isotopic compositions ranged from
0 to 473 mg kg^{-1} soil and from −56.5‰ to 277.1‰, respectively. For both tracers, the concentrations found in soil were
345   considerably smaller than the original concentration of the labelled stemflow water, with the maximum measured in soil
samples representing 9.5% and 55.4% of their original concentrations for Brilliant Blue FCF and deuterium, respectively. This
can be explained by (1) sorption of Brilliant Blue FCF on the trunk bark and soil surfaces and (2) dilution of the stemflow
water by residual soil water.

Both tracers correlated significantly ($p < 0.01$; $R^2 = 0.78$; Figure S5): there was no evidence that deuterium moved deeper or
350   farther through the soil than the dye tracer. This suggests that the two tracers could be used indifferently to delineate preferential
flow pathways. It is known that Brilliant Blue FCF sorbs to soil surfaces and is therefore retarded to some extent (Flury &
Flühler, 1995), but the close correlation of Brilliant Blue FCF with deuterium in our study shows that the stemflow water was
mainly moving along preferential flow pathways with minimal interactions with adsorbing surfaces.

The water samples taken from the mini-piezometer revealed that the temporary perched water tables have a similar Brilliant
355   Blue FCF concentration as the original stemflow water of ~5 g L^{-1} (Table S2). This corroborates the prevalence of preferential
flow of the stemflow water once it infiltrates into the soil. However, deeper groundwater (> 1 m depth) did not show the
presence of dye or deuterium enrichment, indicating that stemflow water did not penetrate deep into the subsoil.

4. Conclusions

Stemflow infiltration occurred in an annulus-shaped area in the vicinity of the trunk and was characterized by high spatio-
360   temporal variability. In some locations, perched water tables developed at shallow depths. Dye patterns and isotopic
composition demonstrated qualitatively and quantitatively the dominance of preferential flow in the soil. The double-
funnelling phenomenon was clearly shown by the infiltration of stemflow into the soil along the surface of coarse roots and
macropore channels. The root architecture was the main driver stemflow water redistribution both horizontally and
vertically in the soil matrix, followed by bypass flow along the macropore network.

365   The dual tracer approach (Brilliant Blue FCF dye and deuterium) together with *in situ* sensing of soil moisture delineates and
quantifies stemflow belowground funnelling very well. Brilliant Blue FCF is an excellent dye tracer to stain and measure
preferential flow pathways. The concentration (5 g L^{-1}) used ensured correctly that mobility would not be limited (despite its
possible sorption by trunk bark and soil surfaces) by the local conditions of the present study (i.e., rough bark and silt loam
soils). On the other hand, deuterium is a conservative tracer, but the preferential flow paths can be identified with extensive
370   soil sampling and analyses.

We can infer from our dye tracing analysis of a single tree that stemflow double funnelling is a dominant hydrological feature
Mediterranean forest catchments. Stemflow infiltration can also contribute to the groundwater recharge by bypass flow,
although we did not directly observe this phenomenon in our study. Although our approach allowed us to investigate the
isolated effect of stemflow on infiltration and soil moisture, we must highlight that other dynamics can be expected when the
375   effect of throughfall is not excluded (as it was in our study), leading probably to a more homogeneous distribution of SWC
around the trunk. Further studies are needed to replicate our approach with more trees and species with different root
architecture and under different prior soil moisture conditions. Simultaneous throughfall tracing (using additional tracers)

should also be included. In addition, the belowground transport and fate of solutes (e.g., pollutants) contained in stemflow water is a related hot topic that also requires future research.

390 **References**

Bargués Tobella, A., Reese, H., Almaw, A., Bayala, J., Malmer, A., Laudon, H., and Ilstedt, U.: The effect of trees on preferential flow and soil infiltrability in an agroforestry parkland in semiarid Burkina Faso, Water Resources Research, 50, 3342-3354, https://doi.org/10.1002/2013WR015197, 2014.

Carlyle-Moses, D. E., Iida, S., Germer, S., Llorens, P., Michalzik, B., Nanko, K., Tischer, A., and Levia, D. F.: Expressing
395 stemflow commensurate with its ecohydrological importance, Advances in Water Resources, 121, 472-479, https://doi.org/10.1016/j.advwatres.2018.08.015, 2018.

Carlyle-Moses, D. E., Iida, S., Germer, S., Llorens, P., Michalzik, B., Nanko, K., Tanaka, T., Tischer, A., and Levia, D. F.: Commentary: What we know about stemflow's infiltration area, Frontiers in Forests and Global Change, 3, 577247, https://doi.org/10.3389/ffgc.2020.577247, 2020.

400 Cayuela, C., Llorens, P., Sánchez-Costa, E., Levia, D. F., and Latron, J.: Effect of biotic and abiotic factors on inter-and intra-event variability in stemflow rates in oak and pine stands in a Mediterranean mountain area, Journal of Hydrology, 560, 396-406, https://doi.org/10.1016/j.jhydrol.2018.03.050, 2018.

Di Prima, S., Giannini, V., Roder, L. R., Giadrossich, F., Lassabatere, L., Stewart, R. D., Abou Najm, M. R., Longo, V., Campus, S., Winiarski, T., Angulo-Jaramillo, R., del Campo, A., Capello, G., Biddoccu, M., Roggero P. P., and Pirastru, M.:
405 Coupling time-lapse ground penetrating radar surveys and infiltration experiments to characterize two types of non-uniform flow, Science of the Total Environment, 806, 150410, https://doi.org/10.1016/j.scitotenv.2021.150410, 2022.

Faé, G. S., Montes, F., Bazilevskaya, E., Añó, R. M., and Kemanian, A. R.: Making soil particle size analysis by laser diffraction compatible with standard soil texture determination methods, Soil Science Society of America Journal, 83, 1244-1252, https://doi.org/10.2136/sssaj2018.10.0385, 2019.

410 Fan, B., Liu, X., Zhu, Q., Qin, G., Li, J., Lin, H., and Guo, L.: Exploring the interplay between infiltration dynamics and Critical Zone structures with multiscale geophysical imaging: A review, Geoderma, 374, 114431, https://doi.org/10.1016/j.geoderma.2020.114431, 2020.

Flury, M. and Flühler, H.: Tracer characteristics of brilliant blue FCF, Soil Science Society of America Journal, 59, 22-27, https://doi.org/10.2136/sssaj1995.03615995005900010003x, 1995.

415 Flury, M. and Wai, N. N.: Dyes as tracers for vadose zone hydrology, Rev. Geophys., 41, 1002, https://doi.org/10.1029/2001RG000109, 2003.

Flury, M., Flühler, H., Jury, W. A., and Leuenberger, J.: Susceptibility of soils to preferential flow of water: A field study, Water Resources Research, 30, 1945-1954, https://doi.org/10.1029/94WR00871, 1994.

Forrer, I., Papritz, A., Kasteel, R., Flühler, H., and Luca, D.: Quantifying dye tracers in soil profiles by image processing,
420 European Journal of Soil Science, 51, 313-322, https://doi.org/10.1046/j.1365-2389.2000.00315.x, 2000.

German-Heins, J. and Flury, M.: Sorption of Brilliant Blue FCF in soils as affected by pH and ionic strength, Geoderma, 97, 87-101, https://doi.org/10.1016/S0016-7061(00)00027-6, 2000.

Ghodrati, M. and Jury, W. A.: A field study using dyes to characterize preferential flow of water, Soil Science Society of America Journal, 54, 1558-1563, https://doi.org/10.2136/sssaj1990.03615995005400060008x, 1990.

425   Gonzalez-Ollauri, A., Stokes, A., and Mickovski, S. B.: A novel framework to study the effect of tree architectural traits on stemflow yield and its consequences for soil-water dynamics, Journal of Hydrology, 582, 124448, https://doi.org/10.1016/j.jhydrol.2019.124448, 2020.

Guo, L., Mount, G. J., Hudson, S., Lin, H., and Levia, D.: Pairing geophysical techniques improves understanding of the near-surface Critical Zone: Visualization of preferential routing of stemflow along coarse roots, Geoderma, 357, 113953,
430   https://doi.org/10.1016/j.geoderma.2019.113953, 2020.

Hao, X., Ball, B. C., Culley, J. L. B., Carter, M. R., and Parkin, G. W.: Soil density and porosity, in: Soil Sampling and Methods of Analysis, Earth Sciences, Environment & Agriculture, edited by: Carter, M. R. and Gregorich, E. G., CRC Press, Boca Raton, FL, USA, 743-759, https://doi.org/10.1201/9781420005271, 2007.

Hatano, R. and Booltink, H. W. G.: Using fractal dimensions of stained flow patterns in a clay soil to predict bypass flow,
435   Journal of Hydrology, 135, 121-131, https://doi.org/10.1016/0022-1694(92)90084-9, 1992.

Hatano, R., Kawamura, N., Ikeda, J., and Sakuma, T.: Evaluation of the effect of morphological features of flow paths on solute transport by using fractal dimensions of methylene blue staining pattern, Geoderma, 53, 31-44, https://doi.org/10.1016/0016-7061(92)90019-4, 1992.

Hildebrandt, A.: Root-Water Relations and Interactions in Mixed Forest Settings, in: Forest-Water Interactions, Ecological
440   Studies (Analysis and Synthesis), edited by: Levia, D. F., Carlyle-Moses, D. E., Iida, S., Michalzik, B., Nanko, K., and Tischer, A., Springer, Cham, Zug, Switzerland, 319-348, https://doi.org/10.1007/978-3-030-26086-6_14, 2020.

Iovino, M., Pekárová, P., Hallett, P. D., Pekár, J., Lichner, Ľ., Mataix-Solera, J., Alagna, V., Walsh, R., Raffan, A., Schacht, K., and Rodný, M.: Extent and persistence of soil water repellency induced by pines in different geographic regions, Journal of Hydrology and Hydromechanics, 66, 360-368, https://doi.org/10.2478/johh-2018-0024, 2018.

445   Johnson, M. S. and Lehmann, J.: Double-funneling of trees: stemflow and root-induced preferential flow, Écoscience, 13, 324-333, https://doi.org/10.2980/i1195-6860-13-3-324.1, 2006.

Kendall, C. and McDonnell, J. J. (Eds.): Isotope Tracers in Catchment Hydrology, Elsevier, Amsterdam, Netherlands, 1998.

Ketelsen, H. and Meyer-Windel, S.: Adsorption of brilliant blue FCF by soils, Geoderma, 90, 131-145, https://doi.org/10.1016/S0016-7061(98)00119-0, 1999.

450   Levia, D. F. and Frost, E. E.: A review and evaluation of stemflow literature in the hydrologic and biogeochemical cycles of forested and agricultural ecosystems, Journal of Hydrology, 274, 1-29, https://doi.org/10.1016/S0022-1694(02)00399-2, 2003.

Levia, D. F. and Germer, S.: A review of stemflow generation dynamics and stemflow-environment interactions in forests and shrublands, Reviews of Geophysics, 53, 673-714, https://doi.org/10.1002/2015RG000479, 2015.

Levia, D. F., Carlyle-Moses, D., and Tanaka, T. (Eds.): Forest Hydrology and Biogeochemistry: Synthesis of Past Research
455   and Future Directions, Springer, Dordrecht, Netherlands, https://doi.org/10.1007/978-94-007-1363-5, 2011.

Liang, W. L., Kosugi, K. I., and Mizuyama, T.: Soil water dynamics around a tree on a hillslope with or without rainwater supplied by stemflow, Water Resources Research, 47, W02541, https://doi.org/10.1029/2010WR009856, 2011.

Llorens, P. and Domingo, F.: Rainfall partitioning by vegetation under Mediterranean conditions. A review of studies in Europe, Journal of Hydrology, 335, 37-54, https://doi.org/10.1016/j.jhydrol.2006.10.032, 2007.

460   Llorens, P., Gallart, F., Cayuela, C., Roig-Planasdemunt, M., Casellas, E., Molina, A. J., Moreno-de las Heras, M., Bertran, G., Sánchez-Costa, E., and Latron, J.: What have we learnt about Mediterranean catchment hydrology? 30 years observing hydrological processes in the Vallcebre research catchments, Geogr. Res. Lett., 44, 475-501, https://doi.org/10.18172/cig.3432, 2018.

Llorens, P., Latron, J., Carlyle-Moses, D. E., Näthe, K., Chang, J. L., Nanko, K., Iida, S., and Levia, D. F.: Stemflow infiltration
465   areas into forest soils around American beech (Fagus grandifolia Ehrh.) trees, Ecohydrology, 15, e2369, https://doi.org/10.1002/eco.2369, 2022.

Luo, Z., Niu, J., Zhang, L., Chen, X., Zhang, W., Xie, B., Du, J., Zhu, Z., Wu, S., and Li, X.: Roots-enhanced preferential flows in deciduous and coniferous forest soils revealed by dual-tracer experiments, Journal of Environmental Quality, 48, 136-146, https://doi.org/10.2134/jeq2018.03.0091, 2019.

470   Metzger, J. C., Wutzler, T., Dalla Valle, N., Filipzik, J., Grauer, C., Lehmann, R., Roggenbuck, M., Schelhorn, D., Weckmüller, J., Küsel, K., Totsche, K. U., Trumbore, S., and Hildebrandt, A.: Vegetation impacts soil water content patterns by shaping canopy water fluxes and soil properties, Hydrological Processes, 31, 3783-3795, https://doi.org/10.1002/hyp.11274, 2017.

Molina, A. J., Llorens, P., Garcia-Estringana, P., de Las Heras, M. M., Cayuela, C., Gallart, F., and Latron, J.: Contributions
475   of throughfall, forest and soil characteristics to near-surface soil water-content variability at the plot scale in a mountainous Mediterranean area, Science of the Total Environment, 647, 1421-1432, https://doi.org/10.1016/j.scitotenv.2018.08.020, 2019.

Pinos, J., Latron, J., Levia, D. F., and Llorens, P.: Drivers of the circumferential variation of stemflow inputs on the boles of Pinus sylvestris L. (Scots pine), Ecohydrology, 14, e2348, https://doi.org/10.1002/eco.2348, 2021.

Poyatos, R., Latron, J., and Llorens, P.: Land use and land cover change after agricultural abandonment, Mountain Research
480   and Development, 23, 362-368, https://doi.org/10.1659/0276-4741(2003)023[0362:LUALCC]2.0.CO;2, 2003.

Rubio, C. M., Llorens, P., and Gallart, F.: Uncertainty and efficiency of pedotransfer functions for estimating water retention characteristics of soils, European Journal of Soil Science, 59, 339-347, https://doi.org/10.1111/j.1365-2389.2007.01002.x, 2008.

Schwärzel, K., Ebermann, S., and Schalling, N.: Evidence of double-funneling effect of beech trees by visualization of flow
485   pathways using dye tracer, Journal of Hydrology, 470, 184-192, https://doi.org/10.1016/j.jhydrol.2012.08.048, 2012.

Spencer, S. A. and van Meerveld, H. V.: Double funnelling in a mature coastal British Columbia forest: spatial patterns of stemflow after infiltration, Hydrological Processes, 30, 4185-4201, https://doi.org/10.1002/hyp.10936, 2016.

Sprenger, M., Llorens, P., Cayuela, C., Gallart, F., and Latron, J.: Mechanisms of consistently disjunct soil water pools over (pore) space and time, Hydrology and Earth System Sciences, 23, 2751-2762, https://doi.org/10.5194/hess-23-2751-2019,
490   2019.

Tischer, A., Michalzik, B., and Lotze, R.: Nonuniform but highly preferential stemflow routing along bark surfaces and actual smaller infiltration areas than previously assumed: A case study on European beech (Fagus sylvatica L.) and sycamore maple (Acer pseudoplatanus L.), Ecohydrology, 13, e2230, https://doi.org/10.1002/eco.2230, 2020.

Van Schaik, N. L. M. B.: Spatial variability of infiltration patterns related to site characteristics in a semi-arid watershed,
495   Catena, 78, 36-47, https://doi.org/10.1016/j.catena.2009.02.017, 2009.

Van Stan, J. T., Gutmann, E., and Friesen, J. (Eds.): Precipitation Partitioning by Vegetation: A Global Synthesis, Springer, Cham, Switzerland, https://doi.org/10.1007/978-3-030-29702-2, 2020.

Van Stan, J. T., Ponette-González, A. G., Swanson, T., and Weathers, K. C.: Throughfall and stemflow are major hydrologic highways for particulate traffic through tree canopies, Frontiers in Ecology and the Environment, 19, 404-410,
500   https://doi.org/10.1002/fee.2360, 2021.

Van Stiphout, T. P. J., Van Lanen, H. A. J., Boersma, O. H., and Bouma, J.: The effect of bypass flow and internal catchment of rain on the water regime in a clay loam grassland soil, Journal of Hydrology, 95, 1-11. https://doi.org/10.1016/0022-1694(87)90111-9, 1987.

Wang, X., Wang, J., and Zhang, J.: Comparisons of three methods for organic and inorganic carbon in calcareous soils of
505   northwestern China, PLOS ONE, 7, e44334, https://doi.org/10.1371/journal.pone.0044334, 2012.

Weiler, M. and Flühler, H.: Inferring flow types from dye patterns in macroporous soils, Geoderma, 120, 137-153, https://doi.org/10.1016/j.geoderma.2003.08.014, 2004.

Yue, K., De Frenne, P., Fornara, D. A., Van Meerbeek, K., Li, W., Peng, X., Ni, X., Peng, Y., Wu, F., Yang, Y., and Peñuelas, J.: Global patterns and drivers of rainfall partitioning by trees and shrubs, Global Change Biology, 27, 3350-3357,
510   https://doi.org/10.1111/gcb.15644, 2021.

Zhang, Y. and Schaap, M. G.: Weighted recalibration of the Rosetta pedotransfer model with improved estimates of hydraulic parameter distributions and summary statistics (Rosetta3), Journal of Hydrology, 547, 39-53, https://doi.org/10.1016/j.jhydrol.2017.01.004, 2017.

515   Zhang, Y., Wang, X., Pan, Y., Hu, R., and Chen, N.: Global quantitative synthesis of effects of biotic and abiotic factors on stemflow production in woody ecosystems, Global Ecology and Biogeography, 30, 1713-1723, https://doi.org/10.1111/geb.13322, 2021.

Zisa, R. P., Halverson, H. G., and Stout, B. B.: Establishment and early growth of conifers on compact soils in urban areas, U.S. Department of Agriculture, Forest Service, Northeastern Forest Experiment Station, Broomall, PA, USA, Res. Pap. NE-451, 8 pp., 1980.

520

525

530

535

540

545

Tables

Table 1. Soil water content measured with TDR probes in different directions around the tree trunk. Pre-stemflow corresponds to t = 0 min and post-stemflow to t = 510 min. Peak SWC is the maximum during the experiment.

Distance/cardinal direction	TDR probe ID	Pre-stemflow SWC (%)	Post-stemflow SWC (%)	Peak SWC (%)	Maximum difference in SWC (%)	Time until peak in SWC (min)
10 cm distance						
north	swc-N10	32	38	42	11	361
northeast	swc-NE10	29	39	45	16	363
east	swc-E10	33	38	41	9	367
southeast	swc-SE10	35	39	40	5	362
south	swc-S10	29	33	34	5	363
southwest	swc-SW10	28	34	37	9	366
west	swc-W10	33	39	44	11	362
northwest	swc-NW10	29	38	44	15	360
30 cm distance						
north	swc-N30	24	30	43	19	363
northeast	swc-NE30	31	35	42	11	366
east	swc-E30	31	34	41	10	365
southeast	swc-SE30	41	42	42	†	†
south	swc-S30	26	29	32	5	369
southwest	swc-SW30	30	31	31	†	†
west	swc-W30	46	46	46	†	†
northwest	swc-NW30	35	38	42	7	381

550   † Denotes no real peak was observed.

555

560

565

Hydrology and
Earth System
Sciences
Discussions
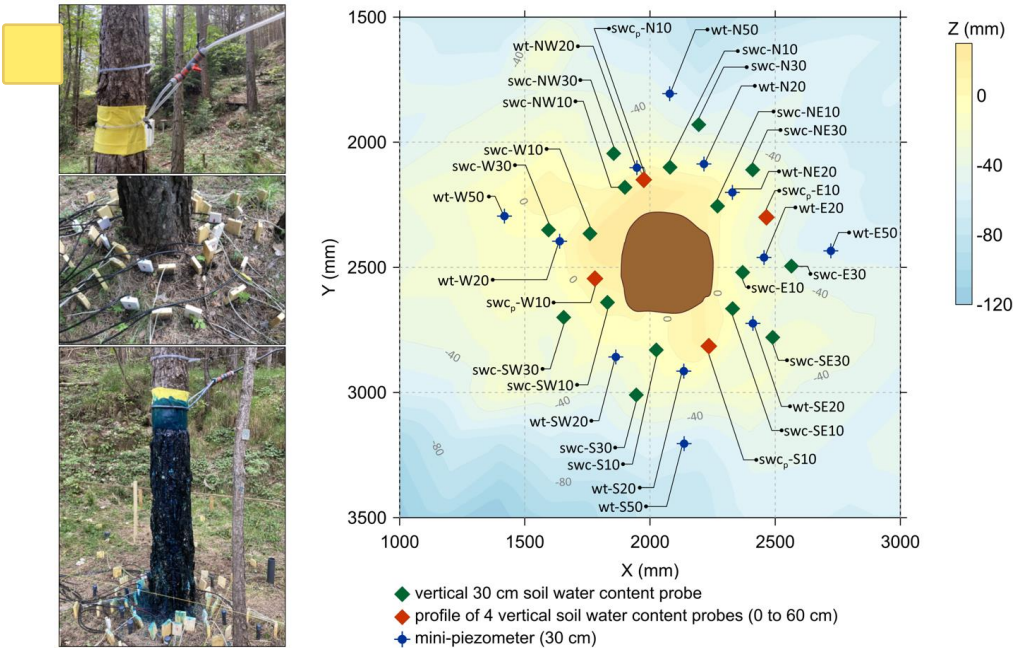Open Access
EGU

Figures

Figure 1. Tracer experiment set-up. Pictures of the artificial stemflow set-up and soil instrumentation before and after (last picture) the tracer experiment. Top view of the experimental area showing microtopography and location of instruments around the selected tree. swc = vertical 30 cm soil water content probe; swc_p = profile of 4 vertical soil water content probes; wt = mini-piezometer (30 cm deep); N = North, E = East, S = South, W = West. The number on the label of each location refers to the distance (cm) from the tree trunk.

590
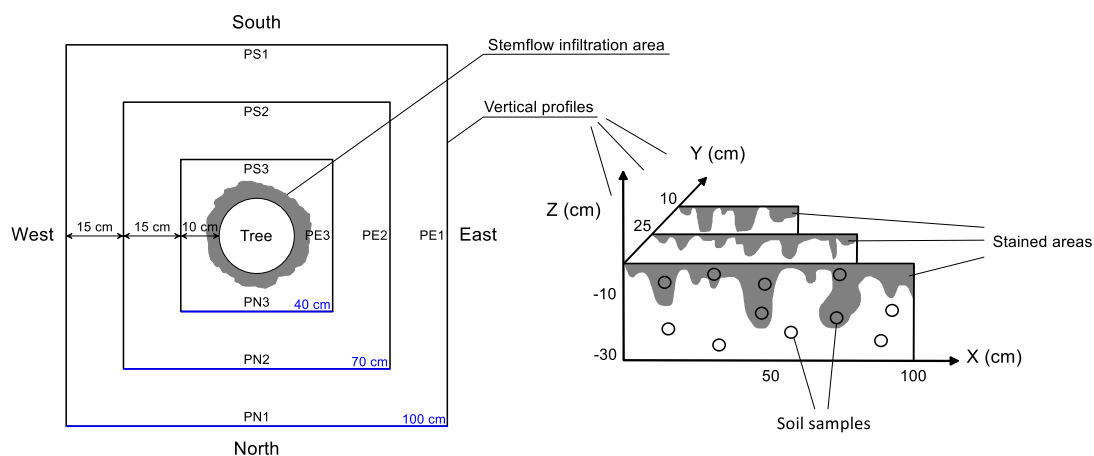
Figure 2. Top and vertical view of the different profiles excavated and the sampling.

595

600

605

610

615

Hydrology and
Earth System
Sciences
Discussions
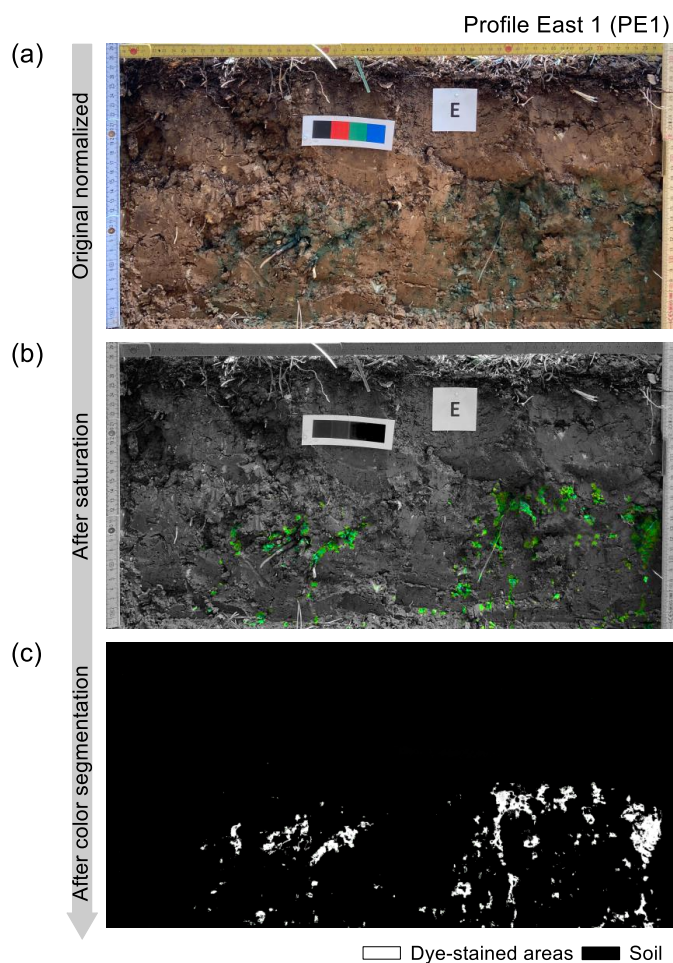
Figure 3. Image analysis procedure of soil profile photographs. (a) Geometric correction, recalibration of colours and illumination, (b) Colour saturation adjustment and (c) Colour segmentation by using a supervised classification.
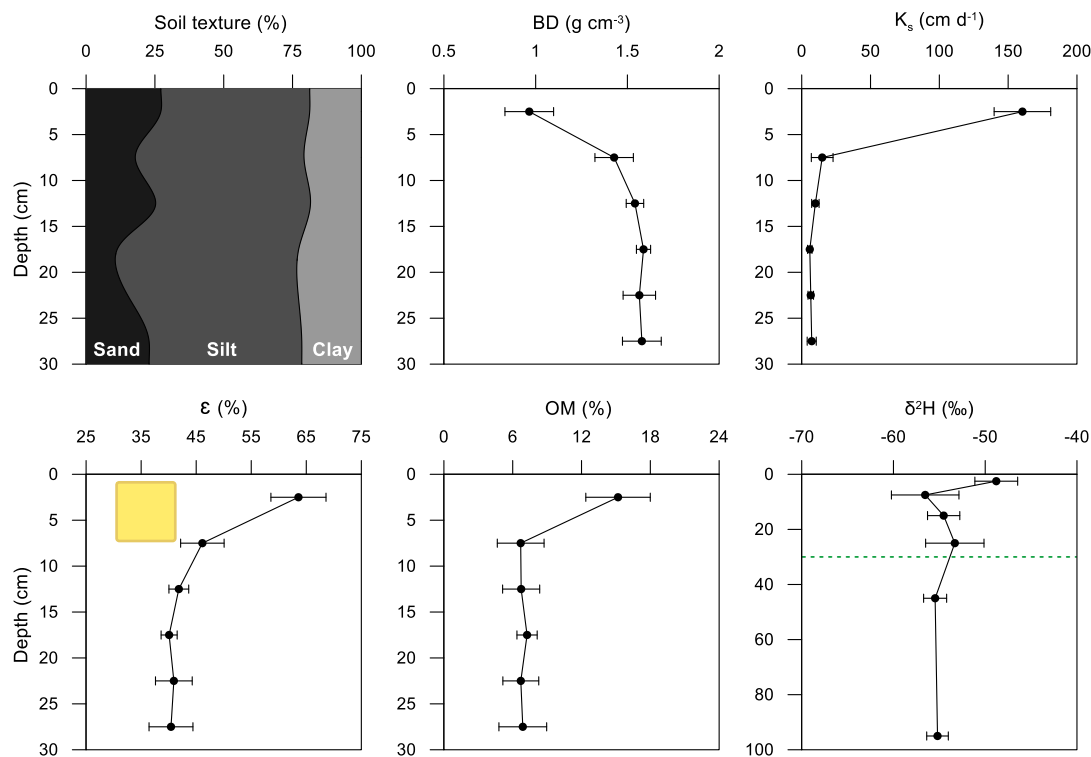
620

625

630

18

Figure 4. Soil physical properties at the pine forest stand. BD = bulk density, K_s = saturated hydraulic conductivity, ε = porosity, OM = organic matter content, $δ^2H$ = deuterium isotopic composition of soil water. Note the different scales of the depth axes for the isotopic composition (the green dotted line is the 30-cm depth). Data represent means and standard deviations (n = 6 for physical properties and n = 4 for isotopic composition).

655
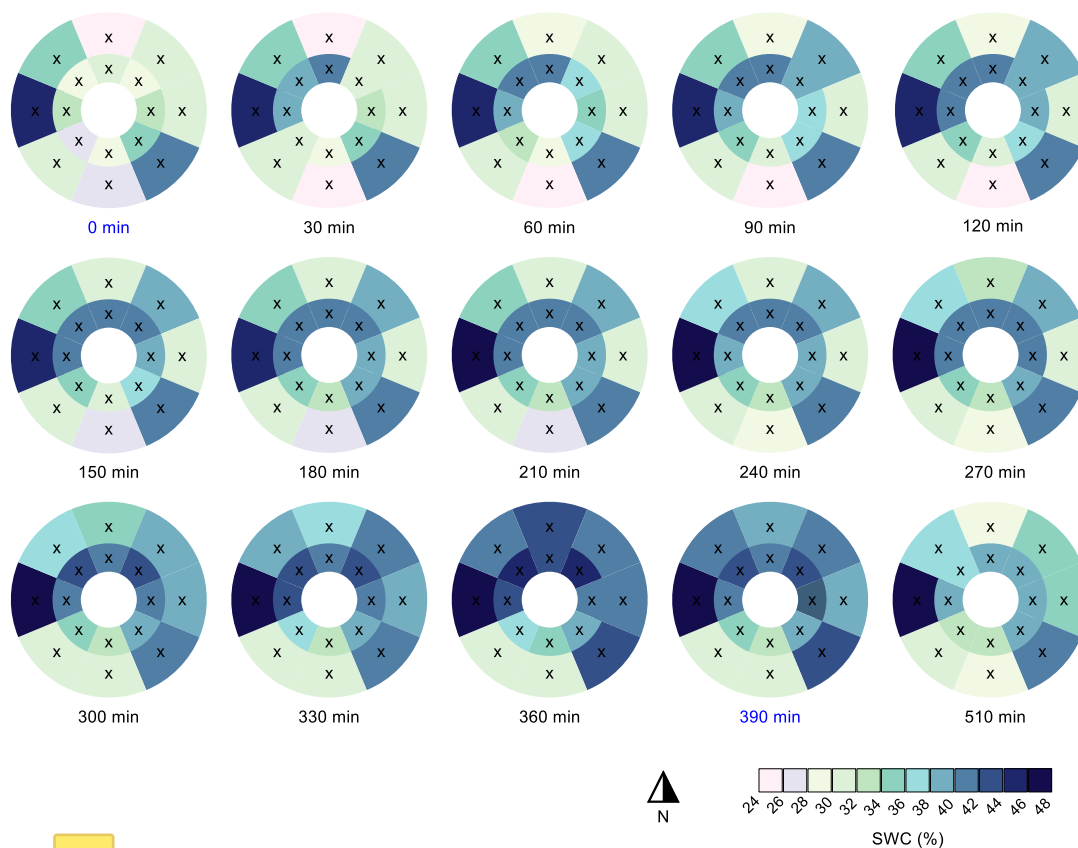
Figu[...] ime series of spatial patterns of volumetric soil water content (SWC) during the experiment. Artificial stemflow was initiated at t = 0 min and stopped after around t = 390 min (highlighted in blue). Cross marks denote TDR sensors (approximate location) and the white circle represents the tree trunk.
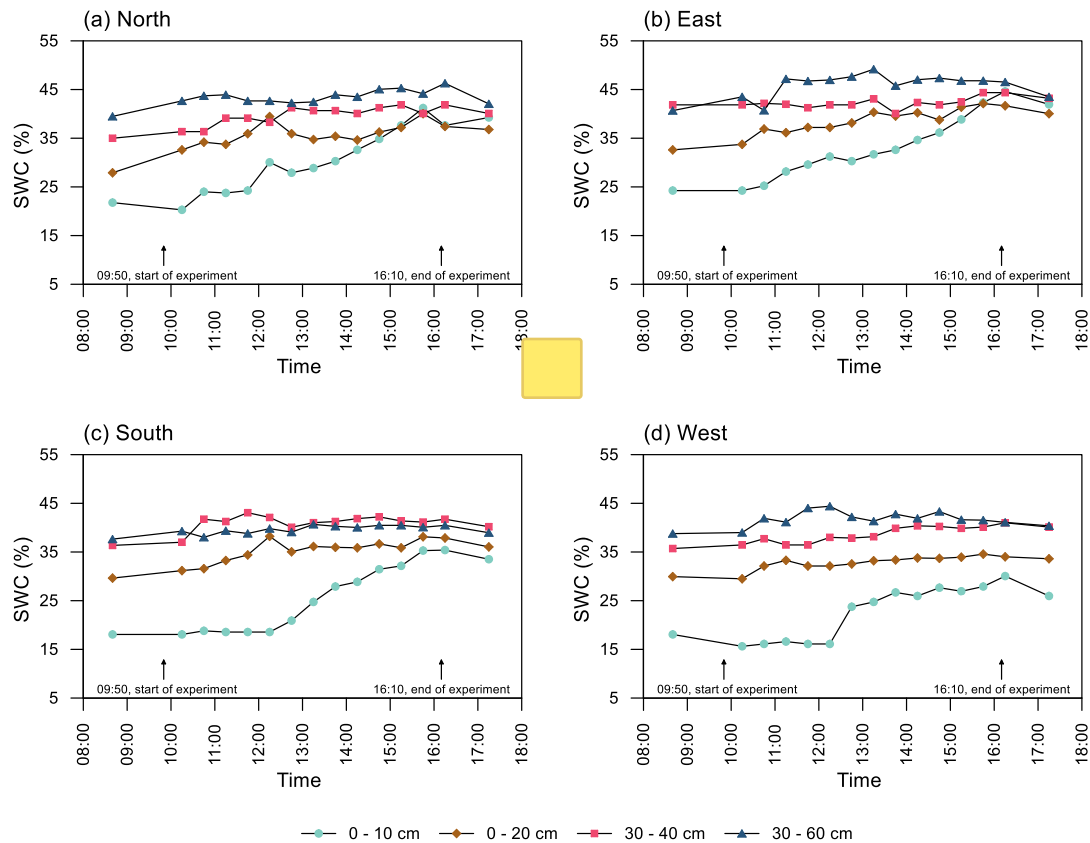
660

665

670

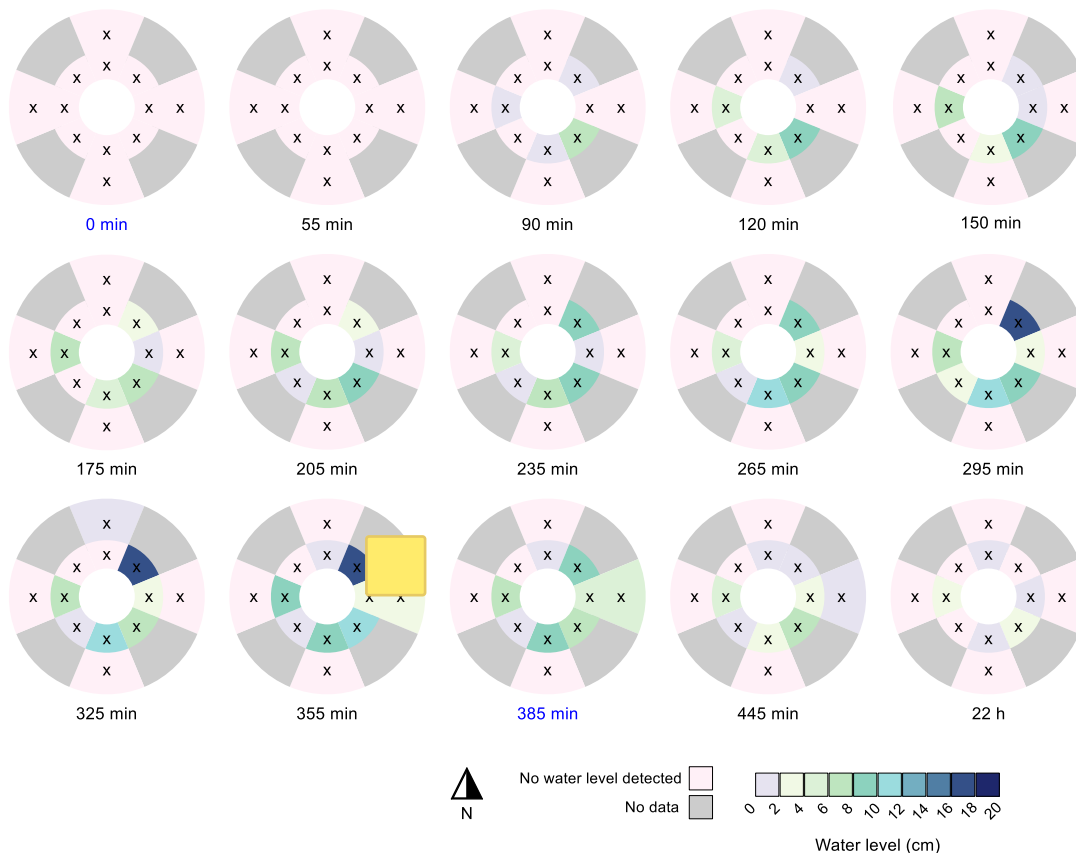**Figure 6.** Temporal evolution of volumetric soil water content (SWC) in depth profiles of each cardinal direction during the stemflow experiment.

Figure 7. Time series of spatial patterns of water level in the 12 mini-piezometers during the experiment. Light pink areas indicate that no water level was detected in the 30-cm deep mini-piezometer, while grey areas indicate zones that were not monitored. Artificial stemflow was initiated at t = 0 min and stopped after around t = 385 min (highlighted in blue). Cross marks denote mini-piezometers (approximate location) and the white circle represents the tree trunk.
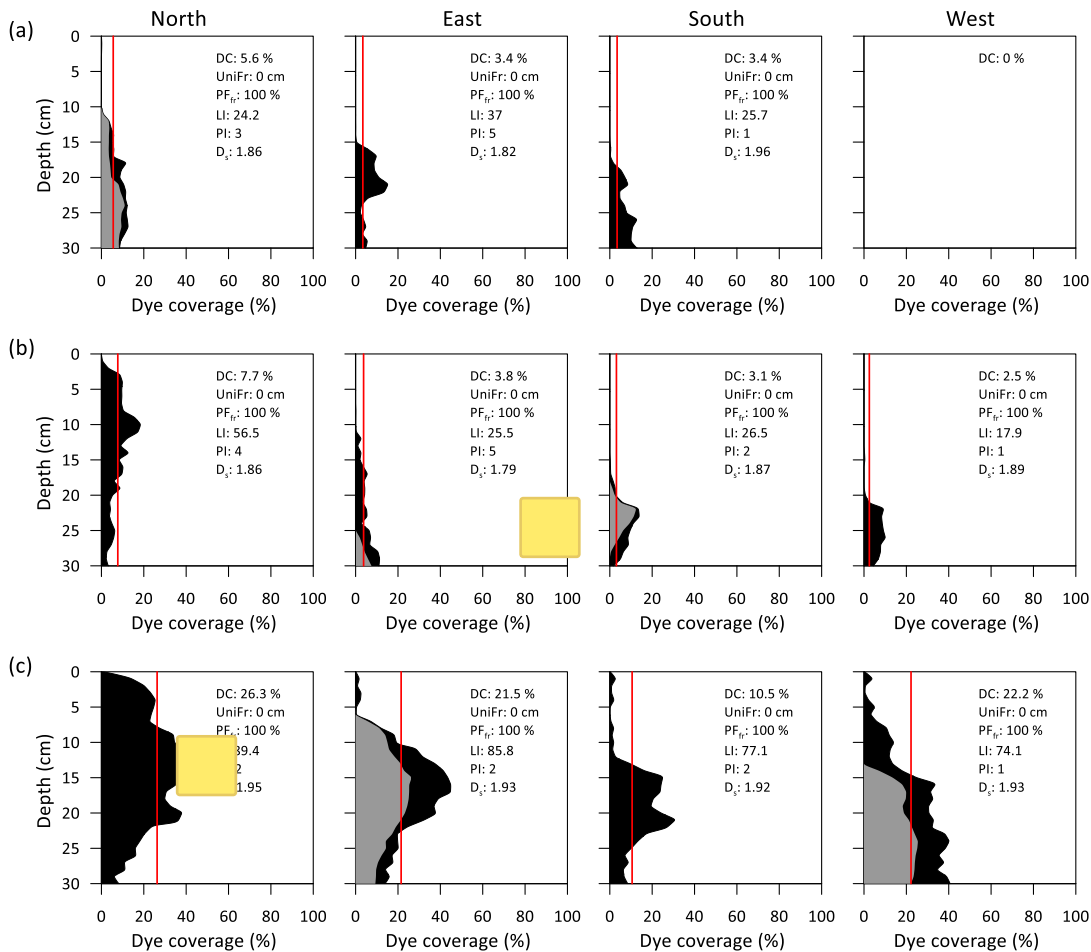
710

Figure 8. Dye coverage (black = soil-stained areas; grey = root-stained areas) of the different soil profiles at a distance of (a) 40 cm, (b) 25 cm and (c) 10 cm from the tree trunk. Root-stained areas refer to the area occupied by stained roots in line with the soil profile. Parameters to quantify the degree of preferential flow are shown within each graph (DC = dye coverage (%), also shown as red line; UniFr = uniform infiltration depth (cm); PF$_{fr}$ = preferential flow fraction (%); LI = length index; PI = peak index; D$_s$= fractal dimension).
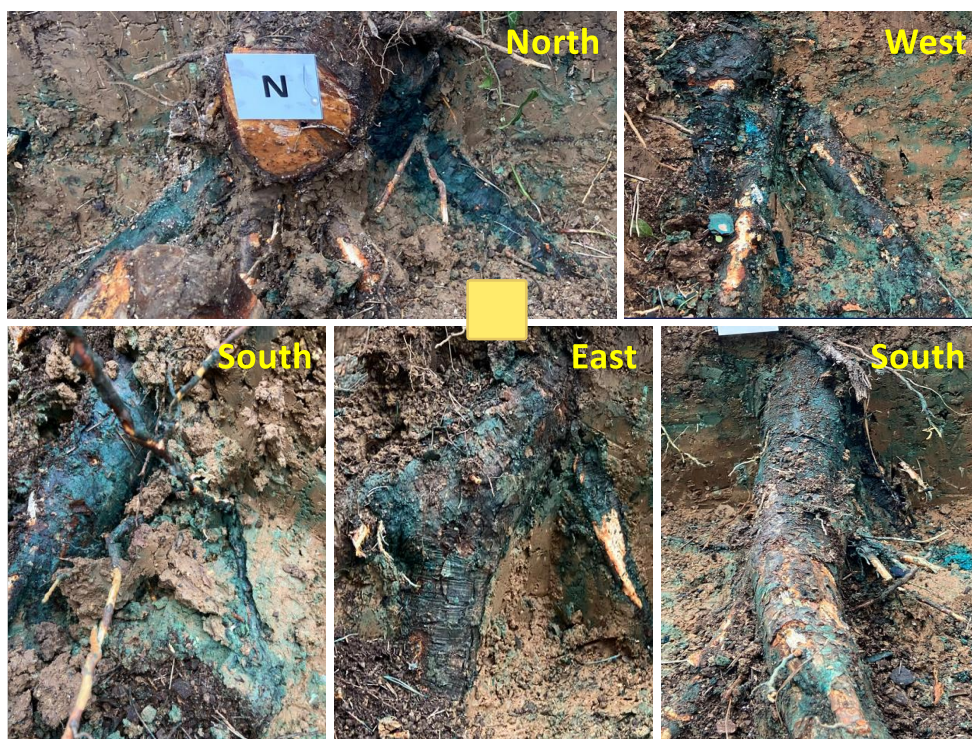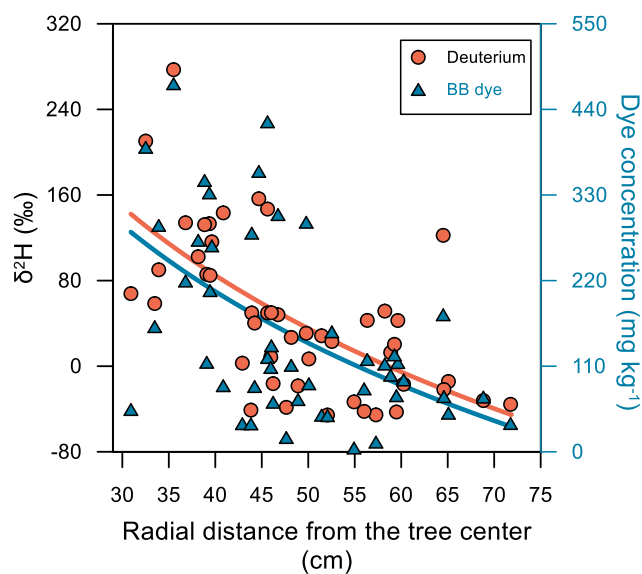
715

720

725

Figure 9. Examples of stained roots observed during excavation of the soil profiles around the tree trunk, illustrating the preferential belowground funnelling of stemflow along coarse roots.

750   **Figure 10.** Relationships between travel distance (three-dimensional coordinate system) with deuterium isotopic composition and Brilliant Blue FCF dye concentration for the 63 soil samples. Solid lines indicate logarithmic fits.